VIP Density Functional Calculations Very Important Paper

How to cite: *Angew. Chem. Int. Ed.* **2022,** *61,* e202211450
International Edition: doi.org/10.1002/anie.202211450
German Edition: doi.org/10.1002/ange.202211450

Mechanistic Origin of Favorable Substituent Effects in Excellent Cu Cyclam Based HNO Sensors

*Yelu Shi, Gianna Stella, Jia-Min Chu, and Yong Zhang**

Abstract: HNO has broad chemical and biomedical properties. Metal complexes and derivatives are widely used to make excellent HNO sensors. However, their favorable mechanistic origins are largely unknown. Cu cyclam is a useful platform to make excellent HNO sensors including imaging agents. A quantum chemical study of Cu cyclams with various substitutions was performed, which reproduced diverse experimental reactivities. Structural, electronic, and energetic profiles along reaction pathways show the importance of HNO binding and a proton-coupled electron transfer mechanism for HNO reaction. Results reveal that steric effect is primary and electronic factor is secondary (if the redox potential is sufficient), but their interwoven effects can lead to unexpected reactivity, which looks mysterious experimentally but can be explained computationally. This work suggests rational substituent design ideas and recommends a theoretical study of a new design to save time and cost due to its subtle effect.

Introduction

HNO confers vasoprotective effects, increases myocardial contractility, and inhibits platelet aggregation.[1] HNO also exerts beneficial effects on ischemia-reperfusion injury,[2] cardiovascular diseases,[3] anti-alcoholism,[4] and antioxidant activity.[5] Sensitive HNO detection methods are critical to help unveil its intriguing biomedical functions. However, most HNO detection methods, though useful in many scientific studies, are indirect or inconvenient for *in vivo* uses.[1a,6] Recently, a number of reaction-based HNO sensors have been developed, utilizing unique structural features such as metals,[7] phosphines,[8] thiols,[9] and ester,[10] many of which can be used *in vivo*.

[*] Dr. Y. Shi, G. Stella, J.-M. Chu, Prof. Dr. Y. Zhang
Department of Chemistry and Chemical Biology, Stevens Institute of Technology
1 Castle Point Terrace, Hoboken, NJ 07030 (USA)
E-mail: yong.zhang@stevens.edu

Although substituents are widely employed in metal complex based HNO sensors,[7] specific roles of substituents that are critical to excellent HNO sensing reactivities have not been explained. For instance, the square planar Cu^{II} cyclam complex offers a useful structural framework to develop HNO sensors, with **CuDHX1** (see Scheme 1) exhibiting a fast near-infrared fluorescence for multi-color in vivo imaging[7g] and a subsequent version CuCLT having improved fluorescent discrimination of HNO and biological thiols.[7l] Further investigation of the substituent effect on the platform of Cu cyclam helped the discovery of additional HNO sensors, including **Cu–Ts** (see Scheme 1) and another complex even exhibiting the first reversible sensing of HNO.[7k] These results clearly show that Cu cyclam is an excellent platform for HNO sensor development. However, although the general phenomena of HNO reaction with these Cu^{II} complexes leading to metal reduction to Cu^{I} and generation of NO [Eq. (1)] were experimentally verified,[7g,k,l] the specific substituent effects which make only some of the studied complexes possess excellent HNO reactivities are still not understood. For instance, although both **CuDHX1** and **Cu–Fl** (which differs from **CuDHX1** by missing the benzyl substituent, see Scheme 1) have sufficiently high redox potentials to oxidize HNO, only **CuDHX1** shows significant fluorescence change upon reacting with HNO, while **Cu–Fl** shows marginal fluorescence increase with HNO and an Electron Paramagnetic Resonance (EPR) silent Cu^{I} species was not detected.[7g] In contrast with this case where an electron-donating group (EDG) benzyl makes a significant difference, **Cu–Me_4** (see Scheme 1) with four

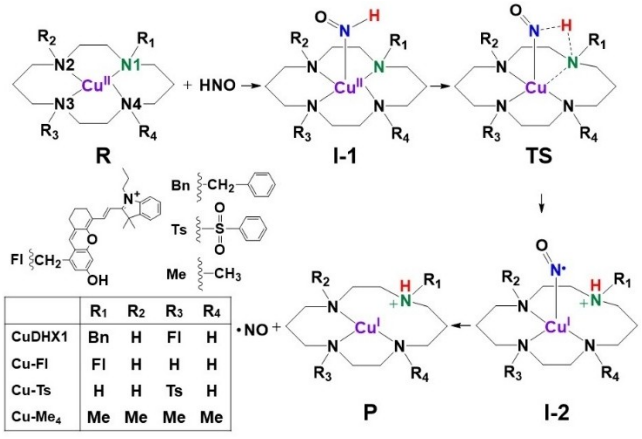

	R_1	R_2	R_3	R_4
CuDHX1	Bn	H	Fl	H
Cu-Fl	Fl	H	H	H
Cu-Ts	H	H	Ts	H
Cu-Me_4	Me	Me	Me	Me

Scheme 1. Schematic pathways of HNO reactions with Cu cyclam complexes. Bn = benzyl; Fl = fluorophore; Me = methyl; Ts = tosyl.

electron-donating methyl groups is unreactive toward HNO, while **Cu**–**Ts** with an electron-withdrawing group (EWG) and the same redox potential has facile HNO reactivity.[7k] Apparently, redox potential is not the only factor needed for HNO reactivity in these redox reactions and a detailed mechanistic study is needed to understand these mysterious substituent effects and reveal important information for future rational design of excellent HNO sensors.

$$Cu^{II} + HNO \rightarrow Cu^{I} + NO + H^{+} \quad (1)$$

In contrast with numerous experimental advances in developing metal-based HNO sensors, there is only one computational reaction mechanism study of such probes,[11] which, however, is for the first metal-based HNO sensor with a non-planar Cu coordination environment and mechanism similar to Cu,Zn-superoxide dismutase (CuZnSOD).[12] Therefore, we performed a quantum chemical computational study of four Cu cyclam complexes in Scheme 1 to elucidate their unknown substituent effects on the complete reaction pathway: from HNO binding to form the first intermediate (**R** + HNO→**I-1**), through HNO conversion (**I-1**→**TS**, transition state →**I-2**) to yield the second intermediate, then NO releasing for final product formation (**I-2**→**P** + NO). This work not only reproduced their distinctive experimental HNO reactivities, but more importantly provided previously unknown mechanistic origins of the substituent effects in excellent HNO sensors.

Results and Discussion

We first studied these Cu cyclam complexes to understand the conformation effect, using the same computational method which recently enabled accurate descriptions of HNO reactivities in metalloproteins and model systems.[11–13] It is known that Cu cyclam complexes commonly exist in the *trans*-III form (a square planar structure with the four nitrogen substituents R_1/R_4 and R_2/R_3 pointing above and below the plane respectively), or the *trans*-I form (another square planar structure featuring all four nitrogen substituents pointing above the plane),[14] see Scheme 2.

Among the four Cu systems in Scheme 1, the latter two have crystal structures (each has two triflate OTf^- counterions): [(Cu–Ts)$(OTf)_2$] and [(Cu–Me_4)$(OTf)_2$]. Energies of the optimized structures show that both prefer the *trans*-III conformation (see Table S1) as found experimentally,[7k] and the predicted Cu–N coordination bond lengths (see Table S2) have a mean absolute deviation (MAD) of 0.029 Å and a mean percentage deviation (MPD) of only 1.4 % (even the three loosely coordinated Cu–OTf distances of 2.6 Å were reproduced with ≈5 % error). These results further support the accuracy of the used computational method.

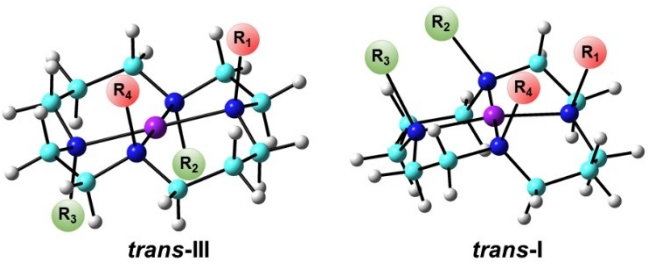

Scheme 2. Cu cyclam *trans*-III and *trans*-I conformations. Atom color scheme: C- cyan, N- blue, H– grey, Cu- purple.

Interestingly, additional calculations show that the *trans*-I conformation is slightly more favorable than the *trans*-III form for **Cu**–**Me_4** alone (without the counterions) and two conformations are of comparable energies (≈0.5 kcal mol^{-1} difference) in the case of **Cu**–**Ts** itself, Table S1. Thus, the preferred conformation may change in the absence of an axial ligand. Since the experimental Cu–OTf bonds are of 2.6–3.9 Å long,[7k] the OTf ligands are labile and easily dissolved in the experimental aqueous solution.

Accordingly, we then studied 4-coordinate **CuDHX1** and **Cu**–**Fl** structures without the labile axial ligand in the solution environment. **CuDHX1** has almost the same Gibbs free energies (ΔG = 0.09 kcal mol^{-1}) for these two conformations, while **Cu**–**Fl** is more favorable in *trans*-III form by ≈2 kcal mol^{-1}, see Table S1.

These results show that both conformations might exist in the solution due to ≲2 kcal mol^{-1} energy differences for these studied Cu cyclams and the relatively preferred conformation may vary depending on different substituents and axial ligands. These features support flexible conformation changes that may be needed for subsequent HNO binding and reaction.

As shown in equation 1, the HNO reactions with these Cu cyclams involve both proton and electron transfer. Experimental work shows that **Cu**–**Me_4** and **Cu**–**Ts** with same redox potentials have no and facile reactivities respectively,[7k] i.e. a dramatic difference indicating that the electron transfer is not through an out-sphere mechanism, but an inner complex - an HNO bound intermediate, which can also facilitate the proton transfer as found in CuZnSOD and its model sensor.[11,12] Therefore, the HNO binding step to form this intermediate is important to be studied for Cu cyclams.

As such, we first examined the HNO bound structures of **Cu**–**Me_4** and **Cu**–**Ts** with both *trans*-I and *trans*-III conformations and with HNO binding to copper on both the same and opposite sides of substituents called *cis* and *trans* respectively here. As shown in Figure S3 and Table S3, none of the *trans* sides can have stable HNO binding as the resultant Cu–N(HNO) distances of all such structures are > 4.2 Å due to steric hindrance. For the *cis* side binding, only *trans*-I conformation has HNO coordination and the sterically less hindered **Cu**–**Ts** has a shorter Cu–N distance (2.426 Å) than **Cu**–**Me_4** (2.854 Å), while the *trans*-III conformation also has no HNO coordination (R_{Cu-N} > 4.4 Å). These results show that the stable HNO binding could only occur with certain conformations from the *cis* side. Then, the relatively favorable *cis* side binding was studied for **CuDHX1** and **Cu**–**Fl** with both *trans*-I and *trans*-III conformations. Interestingly, for these two Cu cyclams, both conformations can coordinate with HNO (R_{Cu-N} = 2.5–

2.9 Å) and the energy differences of <0.5 kcal mol^{-1} are insignificant, see Table S3. The Cu–N distances show that the less crowded substitution in **Cu**–**Fl** than **CuDHX1** leads to shorter/stronger HNO binding in each conformation. These data clearly indicate the importance of steric effect of substitution on HNO binding.

Based on the above investigation, for **Cu**–**Ts** and **Cu**–**Me$_4$**, we then chose the *trans*-I conformation results in the subsequent HNO reaction studies because only this conformation has the HNO bound intermediate. For **CuDHX1** and **Cu**–**Fl**, because both conformations have similar stabilities of the HNO bound intermediates, both were studied. However, as shown in sections 5 and 6 in Supporting Information, the reaction pathways with the *trans*-III conformations are thermodynamically more favorable and kinetically more feasible for both **CuDHX1** and **Cu**–**Fl**, thus the *trans*-III conformation results were used here in the subsequent HNO reaction mechanism study.

It is interesting to note that the HNO binding Gibbs free energies of **CuDHX1**, **Cu**–**Fl**, and **Cu**–**Me$_4$** which have EDGs are around 10–13 kcal mol^{-1}, much higher than that for **Cu**–**Ts** with an EWG, 6.81 kcal mol^{-1}, see Table 1. The binding enthalpies also show that **Cu**–**Ts** has the strongest HNO binding. The Cu–N distance of 2.4 Å in HNO bound intermediate (**I-1**) in **Cu**–**Ts** is accordingly the shortest, see Table 2. This may not be surprising since the EWG can enhance Cu's electron affinity toward the electron-rich substrate HNO. As a result, the bound HNO transfers the most (negative) charge to Cu in **Cu**–**Ts** compared to other Cu cyclams and consequently **Cu**–**Ts**–**I-1** has the least positive Cu charge and the least negative NO charge. This suggests that beyond the steric effect, the electronic effect of a substituent may also play a significant role on HNO binding. In fact, both **Cu**–**Ts** and **Cu**–**Fl** bear the smallest number of substituents and thus similarly least steric effect, but since Ts group is an EWG, unlike Fl in **Cu**–**Fl**, **Cu**–**Ts** has a more favorable binding energy than **Cu**–**Fl**. With both favorable steric and electronic effects, **Cu**–**Ts** has the most stable HNO bound intermediate, see Table 1.

In contrast, **Cu**–**Me$_4$** with the most substituents and thus the highest steric effect plus an unfavorable electronic effect here is associated with the greatest binding energy (ΔG of 12.52 kcal mol^{-1}). In fact, this is the only Cu cyclam studied here possessing a positive binding electronic energy ΔE (see Table 1), which means that even the electronic interaction between HNO and **Cu**–**Me$_4$** is unstable and thus there is no stable HNO bound intermediate for this system. Compared with **Cu**–**Me$_4$** displaying no experimental HNO reactivity, the other three Cu cyclams with HNO reactivities all have negative binding electronic energies (see Table 1). These

Table 1: Reaction Energies in Each Step (unit: kcal mol^{-1}).

System	Step	ΔE	ΔE_{ZPE}[a]	ΔH	ΔG
CuDHX1	**R+HNO→I-1**	−0.80	0.38	0.59	9.84
	I-1→ I-2	−4.84	−3.94	−3.93	−4.01
	I-2→P+NO	−1.28	−2.91	−3.26	−13.21
Cu–Fl	**R+HNO→I-1**	−1.77	−0.09	−0.15	10.96
	I-1→I-2	1.43	1.45	1.20	−0.33
	I-2→P+NO	−0.68	−1.7	−1.17	−10.88
Cu–Ts	**R+HNO→I-1**	−4.93	−3.36	−3.42	6.81
	I-1→I-2	−2.07	−1.66	−1.67	−2.07
	I-2→P+NO	0.66	−0.06	0.28	−9.69
Cu–Me$_4$	**R+HNO→I-1**	0.56	2.24	2.18	12.52
	I-1→I-2	−6.77	−5.91	−5.97	−5.65
	I-2→P+NO	2.37	0.98	1.16	−8.64

[a] Zero-point energy corrected electronic energy.

Table 2: Relative Energies,[a] Key Geometric Parameters, Spin Densities, and Charges.

Species	ΔE [kcal mol^{-1}]	ΔE_{ZPE} [kcal mol^{-1}]	ΔH [kcal mol^{-1}]	ΔG [kcal mol^{-1}]	R_{Cu-N} [Å]	R_{H-N} [Å]	$R_{H\cdots N1}$ [Å]	R_{Cu-N1} [Å]	$\rho^{\alpha\beta}{}_{Cu}$ [e]	$\rho^{\alpha\beta}{}_{NO}$ [e]	Q_{Cu} [e]	Q_{NO} [e]
CuDHX1–I-1	0.00	0.00	0.00	0.00	2.936	1.045	4.475	2.111	0.474	0.000	1.035	−0.216
CuDHX1–TS	21.61	20.31	19.86	20.59	2.083	1.059	1.897	3.136	0.463	0.111	0.937	−0.217
CuDHX1–I-2	−4.84	−3.94	−3.93	−4.01	2.269	2.082	1.027	3.153	−0.047	1.062	0.630	−0.071
Cu–Fl–I-1	−0.97	−0.47	−0.74	1.12	2.650	1.046	4.231	2.133	0.500	0.001	0.981	−0.222
Cu–Fl–TS	19.2	18.66	17.98	19.96	2.087	1.049	2.091	3.183	0.502	0.080	0.935	−0.167
Cu–Fl–I-2	0.46	0.98	0.46	0.79	2.259	2.138	1.028	3.031	−0.041	1.054	0.600	−0.056
Cu–Ts–I-1	−4.13	−3.74	−4.01	−3.03	2.426	1.044	4.341	2.064	0.521	0.003	0.935	−0.196
Cu–Ts–TS	20.69	19.33	18.63	20.50	2.053	1.078	1.831	2.996	0.457	0.181	0.887	−0.209
Cu–Ts–I-2	−6.20	−5.40	−5.68	−5.10	2.159	2.381	1.023	3.130	−0.020	1.030	0.561	−0.028
Cu–Me$_4$–I-1	1.36	1.86	1.59	2.68	2.854	1.048	4.133	2.107	0.461	0.000	1.117	−0.255
Cu–Me$_4$–TS	19.81	19.34	18.30	21.70	2.034	1.063	1.849	3.078	0.422	0.134	0.999	−0.228
Cu–Me$_4$–I-2	−5.41	−4.05	−4.38	−2.97	2.096	2.121	1.026	3.347	−0.126	1.206	0.729	−0.191

[a] Energies are relative to **CuDHX1–I-1**'s reaction energy in the pathway.

results again highlight the importance of the formation of a stable HNO bound intermediate for subsequent reaction. In fact, a stable HNO bound intermediate also exists in the CuZnSOD reaction with HNO.[12] Although **CuDHX1** and **Cu–Fl** have electron-donating substituents that are electronically unfavorable for HNO binding, they still have HNO bound intermediates due to moderate steric effects from two and one substituents. These results suggest that steric effect is the dominant factor for HNO binding, while electronic effect is secondary and may also be employed to further enhance HNO binding as in the case of **Cu–Ts** discussed above. The reason that the electronic effect is not strong here is probably a result of the fact that HNO binding is weak, with ≈2.4–2.9 Å Cu–N distances.

After the HNO bound **I-1** is formed, a redox reaction occurs to yield Cu^{I} and NO, see equation 1. In addition, HNO's proton is transferred to the nearby proton acceptor. In CuZnSOD, the proton accepting site is a negatively charged histidine ligand,[12] which clearly has a stronger proton affinity than the neutral coordinating histidine ligands. Since the nearby nitrogen sites in Cu cyclams are all neutral, a systematic study of possible protonation sites in cyclams was performed. For **CuDHX1**, the reaction products with protons at each of the four coordinating nitrogens were optimized, which show that N1 with the electron-rich Bn substituent has the lowest energy and N3 which has the electron-donating Fl group is only higher by ≈3 kcal mol^{-1} and significantly more stable than the non-substituted N2/N4 sites by ≈10 kcal mol^{-1}, Table S4. Therefore, the nitrogens with Bn and Fl groups are the preferred protonation sites respectively for **CuDHX1** and **Cu–Fl**. For **Cu–Ts**, the nearby sulfonyl oxygen was also included in the protonation study. As seen from Table S5, N3 with the electron-withdrawing Ts substituent has the highest energy among all nitrogens (which are all better than the oxygen site to accept the proton), while its opposite site N1 has the most favorable protonation. Therefore, these preferred protonated species were used in the following reaction study. For **Cu–Me$_4$**, the four nitrogens are symmetric.

Investigation of the **TS** connecting **I-1** and **I-2** (see Scheme 1 for a general reaction pathway with optimized molecular structures in Figure 1) shows that a proton-coupled electron transfer (PCET) mechanism operates here for all these Cu cyclams, analogous to HNO to NO conversion by the other metal complex[11] and metalloproteins including both heme proteins[13c] and the non-heme

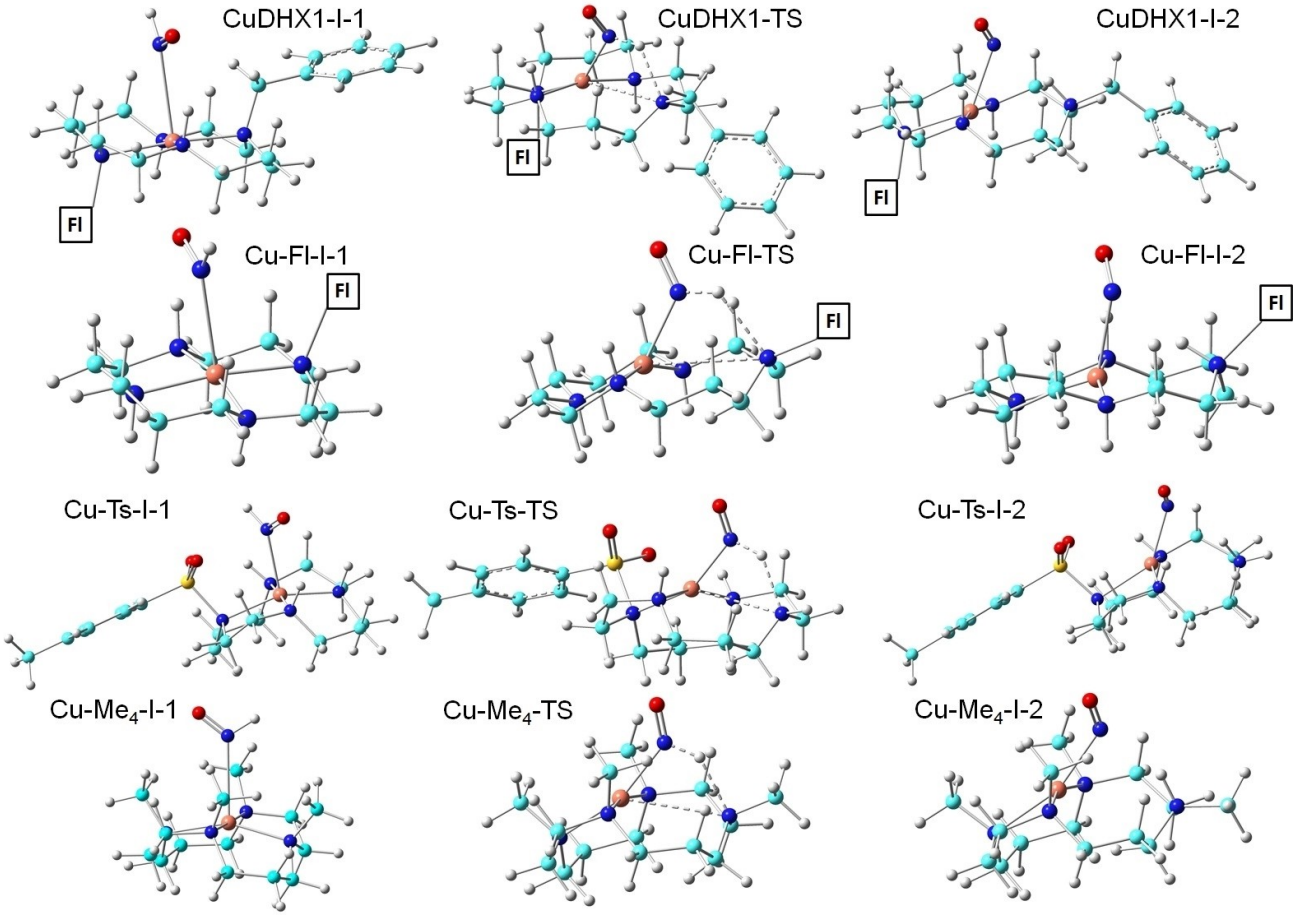

Figure 1. Optimized structures of species in the HNO to NO conversion step by Cu cyclams. Atom color scheme: C- cyan, N- blue, O- red, S- yellow, H- grey, Cu- orange. The Fl group is represented by its symbol for clarity with complete optimized structures in Figure S7. Dash line: bond in transition.

protein.[12] For example, in **CuDHX1**, there is a simultaneous electron transfer as indicated by the spin density results of NO ($\rho^{\alpha\beta}_{NO}$) increasing from 0 e in **I-1** to 0.1 e in **TS** then to ≈1.0 e in **I-2**, and accordingly Cu ($\rho^{\alpha\beta}_{Cu}$) decreasing from 0.47 e in **I-1** to 0.46 e in **TS** then to ≈0 e in **I-2**, and the proton transfer as seen from the H–NO bond length elongation from 1.045 Å in **I-1** to 1.059 Å in **TS** then to 2.082 Å in **I-2**, and the H–N1 distance shortening from 4.475 Å in **I-1** to 1.897 Å in **TS** then to 1.027 Å in **I-2**. Namely, a hydrogen bond is formed between H and N1 at **TS** (this also occurs for other Cu cyclams, as indicated by 1.8–2.1 Å H···N1 distances in Table 2) to facilitate the proton transfer, which is absent in **I-1** ($R_{H\cdots N1}$ > 4 Å, Table 2) since N1′s lone pair forms the coordination bond with Cu and thus is unavailable for hydrogen bonding. The proton transfer breaks the Cu–N1 coordination bond, see bond lengths of ≈2.1 Å in **I-1** to ≈3.1 Å in **TS** and ≈3.2 Å in **I-2** (Table 2), which makes N1 ready for the hydrogen bond with the incoming proton at **TS**. The qualitative reaction features of a barriered PCET and loss of one Cu coordination bond upon completion of proton transfer are identical to the first step of the native CuZnSOD reaction[15] and the HNO to NO reactions mediated by CuZnSOD[12] and its model.[11] However, quantitatively the reaction barrier from **I-1** to **TS** via CuZnSOD is lower than here by ≈9 kcal mol^{-1}, which may be a result of 1) a more flexible non-planar coordination environment in the protein and thus a lower energy cost for breaking the Cu–N1 bond (≈1 Å elongation from **I-1** to **TS** for Cu cyclams vs. only ≈0.4 Å elongation for CuZnSOD[12]) and 2) a stronger proton acceptor via the negatively charged coordinating histidine ligand in CuZnSOD than the neutral ligand here to reduce the proton transfer energy cost.

Apart from the above-mentioned geometric changes, the Cu–N distance undergoes a significant contraction (≈0.4–0.9 Å) for the forward barrier step **I-1**→**TS**, see Figure 2.

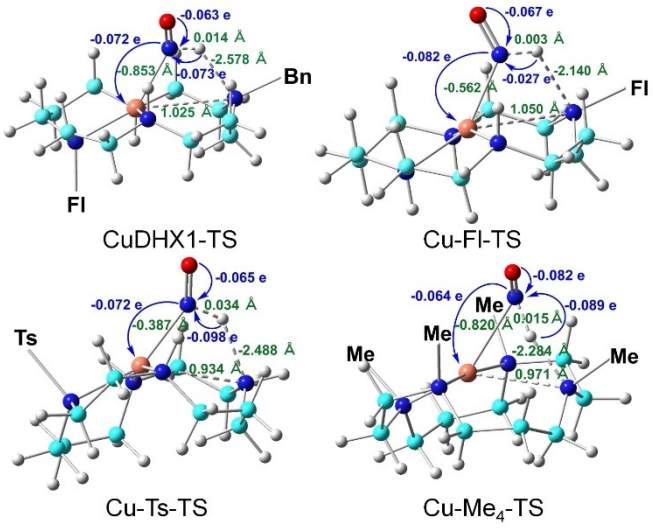

Figure 2. Atomic charge transfer for HNO (in blue) and key bond length changes (in green) from **I-1** to **TS** for Cu cyclams drawn on the **TS** structures.

The charge analysis reveals that a negative charge of ca. 0.07 e was transferred from HNO to Cu in this step, consistent with the electron transfer direction. The absolute charge transfer value trend of **Cu**–**Me$_4$** < **Cu**–**Ts** ≈ **CuDHX1** < **Cu**–**Fl** is inversely correlated with the Gibbs free energies of activation ($\Delta G^{\ddagger}$, **I-1**→**TS**) trend of **Cu**–**Me$_4$** > **Cu**–**Ts** ≈ **CuDHX1** > **Cu**–**Fl**, although both ranges are small. To facilitate the comparison among the studied four Cu cyclams, all energies in this step shown in Table 2 and Figure 3 are with respect to the **I-1**′s reaction energy for **CuDHX1**, which was chosen because it is the only experimental system studied here with fluorescence based HNO detection and imaging.[7g,k] **Cu**–**Me$_4$** which bears the most sterically hindered substitutions has the largest $\Delta G^{\ddagger}$ (see Table 2), while the other three cyclams with one or two substituents have similar barriers within 0.63 kcal mol^{-1} differences. This highlights the substituent's steric effect on the barrier.

It should be noted that although it takes some energies to generate **I-1**, the experimental uses of 50:1 or even 100:1 ratio of HNO donor vs. Cu cyclam[7g,k] can significantly enhance the thermodynamic driving force for its formation especially in the cases of **CuDHX1**, **Cu**–**Fl**, and **Cu**–**Ts**, where a stable **I-1** exists. This facilitates the accumulation of **I-1** as the starting point for the HNO reaction and makes $\Delta G^{\ddagger}$ of **I-1**→**TS** the effective overall barrier for such experimental reactions. Since their $\Delta G^{\ddagger}$ values of ≈20 kcal mol^{-1} are close to some room temperature reactions,[16] these kinetically feasible barriers support their experimentally observed reactivities. However, for **Cu**–**Me$_4$** which does not have a stable **I-1** as found in the previous section, the high **TS** barrier from the starting reactant of 31.54 kcal mol^{-1} (see Table S10) accounts for its experimental inactivity toward HNO.

The reaction energies of this HNO to NO conversion step (**I-1**→**I-2**) are all negative (< −2 kcal mol^{-1}) and thus thermodynamically favorable, except for **Cu**–**Fl** which is almost thermodynamically neutral (ΔG = −0.33 kcal mol^{-1}). **Cu**–**Fl** is also the only Cu cyclam studied here to possess a

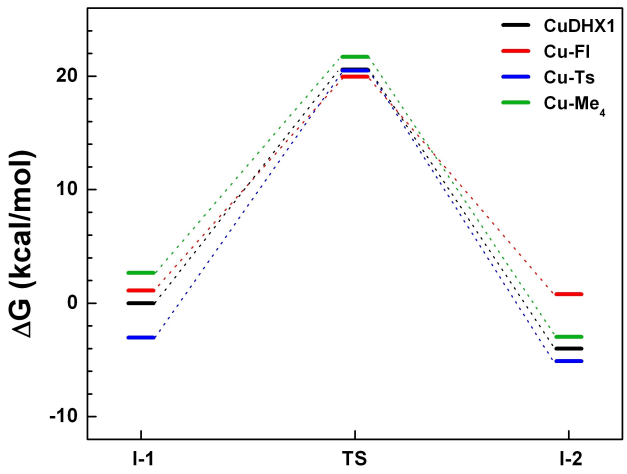

Figure 3. Gibbs free energies along the HNO to NO conversion pathways via Cu cyclams.

positive enthalpy change for this reaction step, see Table 1. These results suggest that the HNO reaction with **Cu–Fl** is reversible or even a little unfavorable regarding ΔH. This feature has not been recognized before and does not favor the formation or accumulation of **I-2** toward final NO releasing to complete the reaction. This helps understand the experimental results: 1) only a tiny fluorescent intensity change of **Cu–Fl** was observed after the addition of the same amount of HNO donors as with **CuDHX1**; 2) an EPR-silent Cu^{I} species was not detected,[7g] unlike the case of **CuDHX1**. The less favorable reaction energy of **Cu–Fl** vs. **CuDHX1** by $\approx$4 kcal mol^{-1} higher (Table 1) is likely due to its relatively less favorable protonation energy by $\approx$3 kcal mol^{-1} in these two sites (Table S4) and its smaller redox potential by 0.045 V[7g] ($\approx$1 kcal mol^{-1}). This indicates that proton transfer is indeed a critical component of the PCET mechanism and a stronger EDG (such as Bn vs. Fl in these two systems) may help make the reaction thermodynamically more favorable.

Above results clearly show that both kinetic barriers and thermodynamic driving forces in the HNO to NO conversion step are important for the various experimental reactivities.

As seen from Table 1, reaction energies of NO releasing step (**I-2**$\rightarrow$**P** + NO) for these Cu cyclams of -9 to -13 kcal mol^{-1} are all much more negative than those in other steps, indicating that this step provides the largest thermodynamic driving force for the overall reaction. This process is largely entropy-driven due to releasing NO gas, unlike the enthalpy-driven HNO to NO conversion step. These features are also similar to the HNO to NO reactions mediated by CuZnSOD[12] and its model.[11]

Combining all steps, it is **CuDHX1** (the only experimentally used HNO fluorescence senor out of these four Cu cyclams) that has the most negative net reaction Gibbs free energy (-7.38 kcal mol^{-1}) and enthalpy (-6.60 kcal mol^{-1}). The extra Bn substituent in **CuDHX1** compared to **Cu–Fl**, although does not help bring down the barrier, plays a crucial role on making its reaction with HNO thermodynamically favorable. In contrast, the net reaction ΔG of -0.25 kcal mol^{-1} and ΔH of -0.12 kcal mol^{-1} for **Cu–Fl**, which are within computational errors to zeros, show that the net reaction is also basically reversible or not thermodynamically favorable, like the HNO to NO conversion step. This is consistent with its poor reactivity with HNO and makes **Cu–Fl** not a practical HNO senor. These results indicate the importance of a strong EDG on the proton acceptor to enhance the proton transfer needed for its PCET reactivity, which helps both the HNO to NO conversion and overall reaction.

Besides the electronic factor, the substituent's steric strain is another key influence on its HNO reactivity. In fact, the main reason **Cu–Me$_4$** with the same sufficiently high redox potential to oxidize HNO as **Cu–Ts**[7k] still exhibits no HNO reactivity is that the steric effect of its tetra-substitution abolishes a stable HNO binding intermediate and leads to a prohibitively high reaction barrier and relatively higher reaction energy, as discussed above. Namely, this steric effect reduces reactivity in every step. In contrast, **Cu–Ts** with an EWG (not a favorable electronic factor) still has facile HNO reactivity, because this system with just one substituent is of little steric hindrance and this EWG enhances the proton affinity of the proton acceptor site opposite to it. This shows that the substituent's steric effect is more important than its electronic nature.

Conclusion

In summary, this first study of substituent effect on metal complex based HNO sensors with various substitution situations reproduced the divergent experimental reactivities, although their reaction mechanisms are common as PCET. More importantly, a detailed theoretical understanding of previously unknown substituent effects was provided, which suggests the following guidelines to facilitate future HNO sensor development:

1) Steric effect is primary. The overcrowding substituents around the reaction center is not preferred. One or two substituents as in the cases of **Cu–Ts** and **CuDHX1** may work.
2) Electronic effect is secondary: both EDG and EWG are good (if it has a sufficient redox potential to oxidize HNO), although the former is better to help the proton transfer. A combination of an EDG and an EWG on opposite sides of the coordination shell that has not been experimentally used before may also work, since this EWG may further enhance the EDG's role on increasing the proton affinity and thus reactivity as for **Cu–Ts**.
3) Substituent effect can be subtle (e.g. an unexpected poor HNO reactivity for **Cu–Fl**, which has only one substituent, least steric effect, and has a favorable EDG and redox potential). Therefore, a theoretical study for a designed case to examine the reaction pathway in detail can help ensure both a favorable kinetic barrier and a favorable thermodynamic reaction energy needed for an excellent HNO sensor before experimental realization, which will save time and cost.

In addition, the comprehensive HNO mechanistic results here may also help investigations of other HNO reactions with metal complexes.

Acknowledgements

This work was supported by an NIH grant GM085774 to YZ.

Conflict of Interest

The authors declare no conflict of interest.

Data Availability Statement

The data that support the findings of this study are available in the supplementary material of this article.

Keywords: Copper · Density Functional Calculations · Nitrogen Oxides · Reaction Mechanisms · Substituent Effects

[1] a) J. M. Fukuto, M. D. Bartberger, A. S. Dutton, N. Paolocci, D. A. Wink, K. N. Houk, *Chem. Res. Toxicol.* **2005**, *18*, 790–801; b) M. D. Bartberger, J. M. Fukuto, K. N. Houk, *Proc. Natl. Acad. Sci. USA* **2001**, *98*, 2194–2198; c) J. C. Irvine, R. H. Ritchie, J. L. Favaloro, K. L. Andrews, R. E. Widdop, B. K. Kemp-Harper, *Trends Pharmacol. Sci.* **2008**, *29*, 601–608; d) J. M. Fukuto, S. Dutton Andrew, N. Houk Kendall, *ChemBioChem* **2005**, *6*, 612–619.

[2] P. Pagliaro, D. Mancardi, R. Rastaldo, C. Penna, D. Gattullo, K. M. Miranda, M. Feelisch, D. A. Wink, D. A. Kass, N. Paolocci, *Free Radical Biol. Med.* **2003**, *34*, 33–43.

[3] a) N. Paolocci, W. F. Saavedra, K. Miranda, M. C. Martignani, T. Isoda, J. M. Hare, M. G. Espey, J. M. Fukuto, M. Feelisch, D. A. Wink, D. A. Kass, *Proc. Natl. Acad. Sci. USA* **2001**, *98*, 10463–11046; b) M. Feelisch, *Proc. Natl. Acad. Sci. USA* **2003**, *100*, 4978–4980; c) K. M. Miranda, T. Katori, C. L. Torres De Holding, L. Thomas, L. A. Ridnour, W. J. McLendon, S. M. Cologna, A. S. Dutton, H. C. Champion, D. Mancardi, C. G. Tocchetti, *J. Med. Chem.* **2005**, *48*, 8220–8228; d) M. Eberhardt, M. Dux, B. Namer, J. Miljkovic, N. Cordasic, C. Will, T. I. Kichko, J. De La Roche, M. Fischer, S. A. Suárez, D. Bikiel, *Nat. Commun.* **2014**, *5*, 4381.

[4] a) E. G. DeMaster, E. Kaplan, F. N. Shirota, H. Nagasawa, T., *Biochem. Biophys. Res. Commun.* **1982**, *107*, 1333–1339; b) E. C. DeMaster, F. N. Shirota, H. T. Nagasawa, *Biochem. Biophys. Res. Commun.* **1984**, *122*, 358–365; c) E. G. DeMaster, F. N. Shirota, H. T. Nagasawa, *Alcohol* **1985**, *2*, 117–121; d) E. G. DeMaster, B. Redfern, H. T. Nagasawa, *Biochem. Pharmacol.* **1998**, *55*, 2007–2015; e) H. T. Nagasawa, E. G. Demaster, B. Redfern, F. N. Shirota, J. W. Goon, *J. Med. Chem.* **1990**, *33*, 3120–3122; f) E. G. Demaster, H. T. Nagasawa, F. N. Shirota, *Pharmacol. Biochem. Behav.* **1983**, *18*, 273–277.

[5] B. E. Lopez, M. Shinyashiki, T. H. Han, J. M. Fukuto, *Free Radical Biol. Med.* **2007**, *42*, 482–491.

[6] a) K. M. Miranda, *Coord. Chem. Rev.* **2005**, *249*, 433–455; b) P. N. Clough, B. A. Thrush, D. A. Ramsay, J. G. Stamper, *Chem. Phys. Lett.* **1973**, *23*, 155–156; c) N. I. Butkovskaya, A. A. Muravyov, D. W. Setser, *Chem. Phys. Lett.* **1997**, *266*, 223–226; d) M. R. Cline, C. Tu, D. N. Silverman, J. P. Toscano, *Free Radical Biol. Med.* **2011**, *50*, 1274–1279; e) M. E. Murphy, H. Sies, *Proc. Natl. Acad. Sci. USA* **1991**, *88*, 10860–10864; f) J. M. Fukuto, A. J. Hobbs, L. J. Ignarro, *Biochem. Biophys. Res. Commun.* **1993**, *196*, 707–713; g) S. A. Suárez, M. A. Marti, P. M. De Biase, D. A. Estrin, S. E. Bari, F. Doctorovich, *Polyhedron* **2007**, *26*, 4673–4679; h) S. I. Liochev, I. Fridovich, *Arch. Biochem. Biophys.* **2002**, *402*, 166–171; i) S. Nelli, M. Hillen, K. Buyukafsar, W. Martin, *Br. J. Pharmacol.* **2000**, *131*, 356–362; j) J. A. Reisz, C. N. Zink, S. B. King, *J. Am. Chem. Soc.* **2011**, *133*, 11675–11685; k) M. R. Cline, J. P. Toscano, *J. Phys. Org. Chem.* **2011**, *24*, 993–998.

[7] a) A. S. M. Islam, M. Sasmal, D. Maiti, A. Dutta, S. Ganguly, A. Katarkar, S. Gangopadhyay, M. Ali, *ACS Appl. Bio Mater.* **2019**, *2*, 1944–1955; b) X. Zhao, C. Gao, N. Li, F. Liu, S. Huo, J. Li, X. Guan, N. Yan, *Tetrahedron Lett.* **2019**, *60*, 1452–1456; c) D. Maiti, A. S. M. Islam, A. Dutta, M. Sasmal, C. Prodhan, M. Ali, *Dalton Trans.* **2019**, *48*, 2760–2771; d) S. Palanisamy, Y.-L. Wang, Y.-J. Chen, C.-Y. Chen, F.-T. Tsai, W.-F. Liaw, Y.-M. Wang, *Molecules* **2018**, *23*, 2551; e) A. Dutta, R. Alam, A. S. M. Islam, A. Dutta, M. Ali, *Dalton Trans.* **2018**, *47*, 11563–11571; f) X. Sun, G. Kim, Y. Xu, J. Yoon, T. D. James, *ChemPlusChem* **2016**, *81*, 30–34; g) A. T. Wrobel, T. C. Johnstone, A. D. Liang, S. J. Lippard, P. Rivera-Fuentes, *J. Am. Chem. Soc.* **2014**, *136*, 4697–4705; h) Y. Zhou, Y.-W. Yao, J.-Y. Li, C. Yao, B.-P. Lin, *Sens. Actuators B* **2012**, *174*, 414–420; i) Y. Zhou, K. Liu, J.-Y. Li, Y. Fang, T.-C. Zhao, C. Yao, *Org. Lett.* **2011**, *13*, 1290–1293; j) J. Rosenthal, S. J. Lippard, *J. Am. Chem. Soc.* **2010**, *132*, 5536–5537; k) S. Kim, M. A. Minier, A. Loas, S. Becker, F. Wang, S. J. Lippard, *J. Am. Chem. Soc.* **2016**, *138*, 1804–1807; l) A. Loas, R. J. Radford, A. D. Liang, S. J. Lippard, *Chem. Sci.* **2015**, *6*, 4131–4140.

[8] a) J. Xu, Y. Bai, Q. Ma, J. Sun, M. Tian, L. Li, N. Zhu, S. Liu, *ACS Omega* **2022**, *7*, 5264–5273; b) H. Niu, X. Mi, X. Hua, Y. Zhang, Y. Zhai, F. Qin, Y. Ye, Y. Zhao, *Anal. Chim. Acta* **2022**, *1192*, 339341; c) C. Zhang, F. He, F. Huang, J. Xu, Y. Hu, *Dyes Pigm.* **2021**, *185*, 108889; d) Z. Chai, D. Liu, X. Li, Y. Zhao, W. Shi, X. Li, H. Ma, *Chem. Commun.* **2021**, *57*, 5063–5066; e) H. Li, C. Wang, L. Cai, X. Yu, L. Wu, N. Yuan, Y. Zhu, N. Jia, T. D. James, C. Huang, *Ind. Eng. Chem. Res.* **2021**, *60*, 15913–15920; f) Z. Li, J. Li, D. Zhang, X. Zhu, Y. Ye, Y. Zhao, *Sens. Actuators B* **2020**, *312*, 127944; g) Z. Liu, Q. Sun, *Spectrochim. Acta Part A* **2020**, *241*, 118680; h) S. Palanisamy, L.-F. Chen, S.-C. Tzou, Y.-M. Wang, *Sens. Actuators B* **2020**, *310*, 127839; i) S. Peng, Z. Li, Y. Zhang, W. Cao, J. Liu, W. Zhu, Y. Ye, *Sens. Actuators B* **2020**, *317*, 128211; j) H. Zhang, Z. Qiao, N. Wei, Y. Zhang, K. Wang, *Talanta* **2020**, *206*, 120196; k) C. Wei, X. Wang, X. Li, X. Jia, X. Hao, J. Zhang, P. Zhang, X. Li, *Spectrochim. Acta Part A* **2020**, *227*, 117765; l) T. Wang, Y. Chai, S. Chen, G. Yang, C. Lu, J. Nie, C. Ma, Z. Chen, Q. Sun, Y. Zhang, J. Ren, F. Wang, W.-H. Zhu, *Dyes Pigm.* **2019**, *166*, 260–265; m) W. An, L. S. Ryan, A. G. Reeves, K. J. Bruemmer, L. Mouhaffel, J. L. Gerberich, A. Winters, R. P. Mason, A. R. Lippert, *Angew. Chem. Int. Ed.* **2019**, *58*, 1361–1365; *Angew. Chem.* **2019**, *131*, 1375–1379; n) K. Zheng, H. Chen, S. Fang, Y. Wang, *Sens. Actuators B* **2016**, *233*, 193–198; o) P. Liu, X. Jing, F. Yu, C. Lv, L. Chen, *Analyst* **2015**, *140*, 4576–4583; p) Z. Miao, J. A. Reisz, S. M. Mitroka, J. Pan, M. Xian, S. B. King, *Bioorg. Med. Chem. Lett.* **2015**, *25*, 16–19; q) H. Zhang, R. Liu, Y. Tan, W. H. Xie, H. Lei, H.-Y. Cheung, H. Sun, *ACS Appl. Mater. Interfaces* **2015**, *7*, 5438–5443; r) X. Jing, F. Yu, L. Chen, *Chem. Commun.* **2014**, *50*, 14253–14256.

[9] a) N. W. Pino, J. Davis, Z. Yu, J. Chan, *J. Am. Chem. Soc.* **2017**, *139*, 18476–18479; b) G. M. Johnson, T. J. Chozinski, D. J. Salmon, A. D. Moghaddam, H. C. Chen, K. M. Miranda, *Free Radical Biol. Med.* **2013**, *63*, 476–484.

[10] Y. Kong, X. Wan, Z. Liu, F. Chen, F. Wu, G. Qin, D. Cao, Y. Cui, *Sens. Actuators B* **2022**, *350*, 130852.

[11] M. A. Michael, G. Pizzella, L. Yang, Y. Shi, T. Evangelou, D. T. Burke, Y. Zhang, *J. Phys. Chem. Lett.* **2014**, *5*, 1022–1026.

[12] Y. Shi, M. A. Michael, Y. Zhang, *Chem. Eur. J.* **2021**, *27*, 5019–5027.

[13] a) E. G. Abucayon, R. L. Khade, D. R. Powell, Y. Zhang, G. B. Richter-Addo, *J. Am. Chem. Soc.* **2016**, *138*, 104–107; b) E. G. Abucayon, R. L. Khade, D. R. Powell, M. J. Shaw, Y. Zhang, G. B. Richter-Addo, *Dalton Trans.* **2016**, *45*, 18259–18266; c) Y. Shi, Y. Zhang, *Angew. Chem. Int. Ed.* **2018**, *57*, 16654–16658; *Angew. Chem.* **2018**, *130*, 16896–16900.

[14] a) R. Ikeda, Y. Soneta, K. Miyamura, *Inorg. Chem. Commun.* **2007**, *10*, 590–592; b) S. L. Hart, R. I. Haines, A. Decken, B. D. Wagner, *Inorg. Chim. Acta* **2009**, *362*, 4145–4151; c) T. H. Lu, W. Z. Shui, S. F. Tung, T. Y. Chi, F. L. Liao, C. S. Chung, *Acta Crystallogr. Sect. C* **1998**, *54*, 1071–1072; d) E. Maimon, I. Zilbermann, G. Golub, A. Ellern, A. I. Shames, H. Cohen, D. Meyerstein, *Inorg. Chim. Acta* **2001**, *324*, 65–72; e) T. J. Lee,

T. Y. Lee, C. Y. Hong, D. T. Wu, C. S. Chung, *Acta Crystallogr. Sect. C* **1986**, *42*, 999–1001; f) J. S. Derrick, Y. Kim, H. Tak, K. Park, J. Cho, S. H. Kim, M. H. Lim, *Dalton Trans.* **2017**, *46*, 13166–13170.

[15] a) V. Pelmenschikov, P. E. M. Siegbahn, *Inorg. Chem.* **2005**, *44*, 3311–3320; b) D. Chen, Q. Wang, H. Zhang, S. Mi, J. Wang, Q. Zeng, G. Zhang, *Int. J. Quantum Chem.* **2010**, *110*, 1394–1401.

[16] a) W. I. Dzik, X. Xu, X. P. Zhang, J. N. H. Reek, B. de Bruin, *J. Am. Chem. Soc.* **2010**, *132*, 10891–10902; b) M. Kazemi, J. Åqvist, *Nat. Commun.* **2015**, *6*, 7293; c) H. Ryu, J. Park, H. K. Kim, J. Y. Park, S.-T. Kim, M.-H. Baik, *Organometallics* **2018**, *37*, 3228–3239.

Manuscript received: August 3, 2022
Accepted manuscript online: September 1, 2022
Version of record online: September 14, 2022